Spin Bottleneck in Resonant Tunneling through Double Quantum Dots with Different Zeeman Splittings

S. M. Huang,[1,2] Y. Tokura,[3,4] H. Akimoto,[1] K. Kono,[1] J. J. Lin,[2] S. Tarucha,[4,5] and K. Ono[1,4,*]

[1]*Low Temperature Physics Laboratory, RIKEN, Wako-shi, Saitama 351-0198, Japan*
[2]*Institute of Physics, National Chiao Tung University, Hsinchu 30010, Taiwan*
[3]*NTT Basic Research Laboratories, NTT Corporation, Atsugi-shi, Kanagawa 243-0198, Japan*
[4]*Quantum Spin Information Project, ICORP-JST, Atsugi-shi, Kanagawa 243-0198, Japan*
[5]*Department of Applied Physics, University of Tokyo, Bunkyo-ku, Tokyo 113-8656, Japan*

We investigated the electron transport property of the InGaAs/GaAs double quantum dots, the electron g factors of which are different from each other. We found that in a magnetic field, the resonant tunneling is suppressed even if one of the Zeeman sublevels is aligned. This is because the other misaligned Zeeman sublevels limit the total current. A finite broadening of the misaligned sublevel partially relieves this bottleneck effect, and the maximum current is reached when interdot detuning is half the Zeeman energy difference.

Electron g factors in III-V semiconductor heterostructures can be tuned by changing the alloy ratio and thickness of each quantum well (QW). Novel spin-related physics in such a g factor-tuned system has attracted considerable interest in the past decade [1]. Electrical tunings of electron g factors has been demonstrated in single and coupled double QWs. The g factor tunings are accomplished by changing the position of the electron wave functions that are spatially delocalized over the regions with different g factors [2]. The g factor tuning used above is a powerful tool for the coherent manipulation of the electron spins; however, these works were done for an ensemble of spins in QWs. To realize the spin-based quantum information devices, which is one of the most ambitious applications of semiconductor spintronics, the coherent manipulation in a single spin level is necessary [3]. The quantum dot (QD) is known as a system where a number of electron as well as their spin state can be well defined and easily controlled [4]. An application of such g factor tuning to QD systems offers a novel candidate for future electric devices for coherent spin manipulation. Tuning the Zeeman splitting of each spin in a QD array has been proposed for individual addressing of spin qubits and fast gate operation between two qubits [3,5]. Selective addressing has been demonstrated so far in a double quantum dot (DQD) made from spatially homogeneous g factors with an additional microferromagnet nearby. The magnet creates a ~ 10 mT field difference of external magnetic field B in each dot [6]. QDs with different g factors can offer a much larger Zeeman energy difference in the same external field with smaller spatial separation.

In this Letter, we report a novel behavior of a single spin in a g factor-tuned DQD, where Zeeman splittings differ greatly from each other in a magnetic field. We investigate this system in a simple, well-defined regime where the total electron number N in the DQD is 0 or 1. Accompanying

the theoretical calculation, we reveal that the resonant tunneling via two Zeeman-split levels is suppressed even if one pair of Zeeman-split levels is aligned. This novel spin bottleneck effect is partially relieved by a finite broadening of QD states owing to interdot and/or dot-electrode tunnel couplings. As a result of competition between the bottleneck and the level broadening effect, the current is maximum in the configuration where interdot level detuning is set to *half* the Zeeman energy difference.

Vertical DQDs with different g factors are formed in a submicron-scale pillar of a triple barrier structure with a surrounding Ti/Au Schottky gate, as schematically shown in the left inset of Fig. 1. The structure consists of a seven-layer structure from top to bottom (or from left to right in the right inset of Fig. 1), a gradiently n-doped $Al_{0.05}Ga_{0.95}As$ source electrode/ $Al_{0.30}Ga_{0.70}As$ (7 nm)/ $In_{0.04}Ga_{0.96}As$ (7.5 nm)/ $Al_{0.30}Ga_{0.70}As$ (6.5 nm)/ GaAs (10 nm)/ $Al_{0.30}Ga_{0.70}As$ (7 nm)/ gradiently n-doped $Al_{0.05}Ga_{0.95}As$ drain electrode. The fabrication procedure is the same with the previous work [7]. Measurements were performed in a dilution refrigerator at an effective electron temperature of ~ 0.1 K and in magnetic fields of up to 15 T applied perpendicular to the wells [8].

Figure 1 shows the differential conductance, dI_{SD}/dV_{SD}, plotted as a function of source-drain voltage V_{SD} and gate voltage V_G in zero magnetic field [9]. Current steps are recognized as dark blue lines. In the positive V_{SD} region, near the current threshold, several current *peaks* (not steps) appear, as marked by arrows. These peaks are due to the resonant tunneling (RT) through the ground state of the left dot and an excited state of the right dot, as shown in the right inset. These current peak lines run nearly parallel to the V_G axis because the side gate capacitively couples to the two dots almost equally, and the alignment of the two-dot levels is nearly maintained against V_G. These behaviors have also been observed in vertical
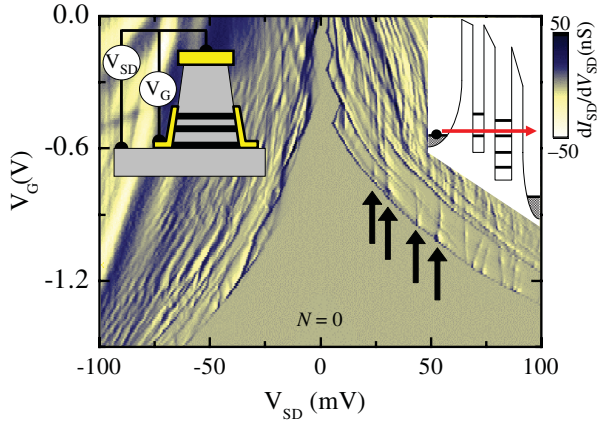
FIG. 1 (color). dI_{SD}/dV_{SD} plot at 0 T. The arrows mark current peaks due to RT where the ground state of left dots is aligned to one of the excited states of the right dot. Left inset: schematic of a gated vertical DQD structure with different g factors for each dot. We apply V_{SD} to the bottom electrode and measure the drain current from the top electrode. Right inset: potential energy landscape for the RT condition.

DQDs [10]. In the first Coulomb staircase defined as the $N = 0$ threshold line and the neighboring parallel line, the current is carried by three charge configurations $(N_1, N_2) = (0,0)$, $(1,0)$, and $(0,1)$, where N_i ($i = 1, 2$) is the number of electron in each dot. In this configuration, it is simple enough to avoid electron-electron interactions in each dot.

Application of the perpendicular magnetic field changes the energies of excited orbital states of the dots and shifts V_{SD} at the RT peak lines [10]. Hereafter, we concentrate on the current peak line found around $V_{SD} \sim 35$ mV and carry out detailed measurements under various magnetic fields. Figures 2(a)–2(d) show the dI_{SD}/dV_{SD} plots for several magnetic fields. The current peak line, which is recognized as adjacent blue and red lines, have a clear kink structure. In vertical DQDs with the same g factor, current peak lines are always straight in any magnetic field, and the kink structure has never been observed. The kink is characterized by two values, δ_1 and δ_2, as marked in Fig. 2(d). Both δ_1 and δ_2 linearly increase with magnetic field, as shown in Figs. 2(e) and 2(f). With low magnetic fields, the peak line becomes straight asymptotically. Similar kink structures are found in all other current peak lines in various positive V_{SD}'s at high magnetic fields, as long as the width of the peak is narrow enough to resolve kinks.

In DQDs with the same g factors, both Zeeman sublevels are aligned at the same time at a certain V_{SD}, regardless of the magnetic field [10]. In DQDs with different g factors, however, the alignment of each Zeeman sublevel is achieved at its own V_{SD}, as schematically shown in Fig. 3, in accordance with the conditions of the measurements. We assign four particular conditions labeled A to D in the magnetic field. Under condition A, the aligned levels for up spin for both dots is in the transport window, and the RT current is carried out by up-spin electrons. By increasing V_G, i.e., by lowering the energy level of both dots, the down-spin Zeeman sublevel in the left dot comes within
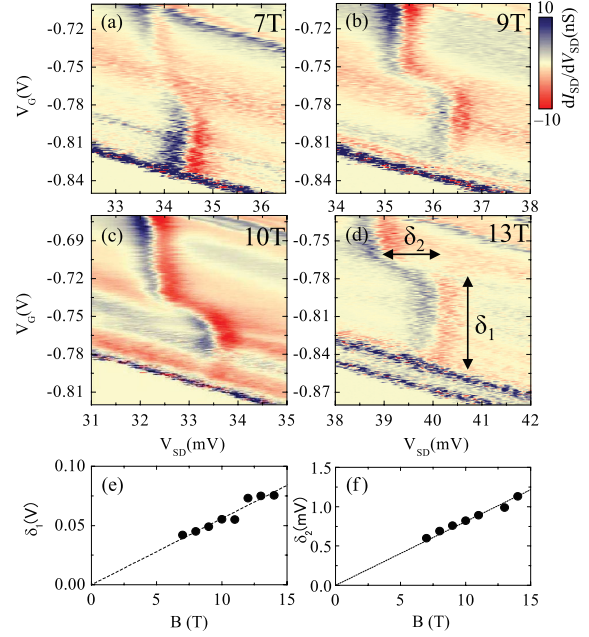

FIG. 2 (color). (a)–(d) Differential conductance, dI_{SD}/dV_{SD}, as a function of V_{SD} and V_G under several different magnetic fields, showing increasing kink structure characterized by δ_1 and δ_2. Magnetic field dependences of (e) δ_1 and (f) δ_2.

the transport window under condition B. Although even the up-spin states are aligned and the RT channel exists, the RT is Coulomb blocked once the down-spin state in the left dot is occupied. We name this suppression process the spin bottleneck. Similarly, under condition C, the occupation of the up-spin in the left dot prohibits the subsequent tunneling even though the aligned down-spin channel exists. Thus, under both conditions B and C, the bottleneck channel is occupied and there is no steady-state resonant current. It should be stressed that this bottleneck effect is similar to the Pauli spin blockade [11] since the stochastic single electron occupation of the bottleneck channel ultimately leads to a blockade in both cases.

The bottleneck can be lifted by level broadening, which is induced by finite tunnel couplings among the dots and the electrodes. The broadening couples the misaligned Zeeman sublevels and provides an escape path for the electron in the bottleneck channel and relieves the bottleneck effect. The electron transport is carried out within the competition between the bottleneck and the escape effects.
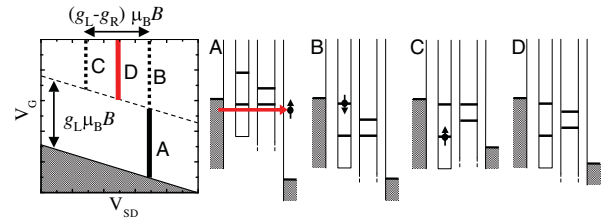

FIG. 3 (color). Schematic diagram of RT peak line for Zeeman mismatched system, and characteristic potential landscapes $A - D$.

While smaller detuning in the RT channel can carry large current, smaller detuning of the bottleneck channel is required to avoid the bottleneck. As a result of the compromise under the intermediate detuning condition D, not under B or C, the maximum current is expected.

This scenario is supported by the theoretical analysis. We evaluated the RT current through two dots with different Zeeman splittings by the Bloch equation method [12,13]. The QD states are described by five bases, $|0,0\rangle$, $|\uparrow,0\rangle$, $|\downarrow,0\rangle$, $|0,\uparrow\rangle$, and $|0,\downarrow\rangle$. Each dot has its own g factor, g_L, and g_R, and their difference is $\Delta = |g_L - g_R|\mu_B B$ (hereafter, we assume $g_L < g_R < 0$). In the calculation, we neglect the cotunneling and tunneling processes with phonon absorption or emission and assume zero temperature. We fix V_{SD} to be large enough so that the right Fermi level is far below the right-dot level ϵ_R. Figure 4(a) shows the differential conductance plotted as a function of $\epsilon_L - \epsilon_R$ and ϵ_L. In the figure, we set the origin of $\epsilon_L - \epsilon_R$ at the position where the lower Zeeman (up-spin) sublevels are aligned and ϵ_L is measured from the Fermi level of the left electrode. There are two conditions labeled case I and case II. In case I, only the up-spin Zeeman sublevel of the left dot is within the transport window (scheme A in Fig. 3). In case II, both the up-spin and down-spin levels of the left dot are within the transport window (schemes $B - D$). In both cases, we obtain a current with a single peak of Lorentzian shape. In case I, the current has a peak at zero interdot detuning. In case II, the maximum current is shifted in the negative detuning direction by the amount of $\Delta/2$. These peak positions in both cases I and II are found to be independent of parameters such as the coupling of the left (right) dot to its neighboring electrode, $\gamma_{L(R)}$, and interdot coupling Ω. Note that $\epsilon_L - \epsilon_R$ and ϵ_L roughly correspond to V_{SD} and V_G in the measurement and δ_1 and δ_2 correspond to $|g_L|\mu_B B$ and $\Delta/2$, respectively. Thus, the clear kink structure in the current peak line in Fig. 4(a) is similar to those in Figs. 2(a)–2(d). Peak currents are plotted in Fig. 4(b) as a function of Ω. The peak current in case II vanishes for small Ω. In contrast, the two peak currents take similar values for large Ω, where the dot-electrode couplings limit the current. In Figs. 2(a)–2(d), the current
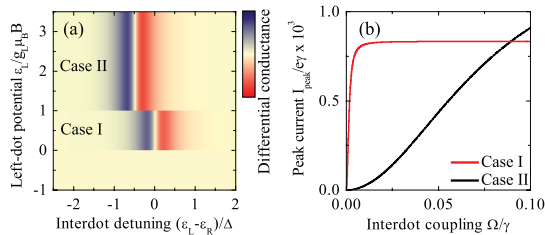
peak heights are almost the same ($\sim$10 pA), both below and above the kink structure. This corresponds to the large Ω. Indeed, our previous studies on vertical DQDs with similar barrier thicknesses indicate $\Omega \sim 0.1$ meV and $\gamma_{L(R)} \lesssim 0.01$ meV [7]. In this sample, γ_L is much smaller than γ_R [9]. In Figs. 2(a)–2(d), transition between the regions corresponds to case I, and II is not as abrupt as in Fig. 4(a) due to the finite temperature. It should be noted that, although this calculation reproduces the shift of the peak and the peak height well, the calculated peak width is always larger than the peak shift $\Delta/2$, whereas in the measurement, $\Delta/2$ seems to be twice as large as the peak width at 13 T. This discrepancy might be solved if we include the cotunneling effect.

In order to convert from δ_1 and δ_2 to $|g_L|\mu_B B$ and $(|g_L - g_R|)\mu_B B$, the voltage drop ratio of three barriers, α_i ($i = 1, 2, 3$), is required. Figure 5(a) shows dI_{SD}/dV_{SD} at 12 T, and we mark L1-L4 for the current threshold lines from the $N = 1$ Coulomb diamond. At the threshold L1, the Fermi energy of the left electrode is aligned with the energy level of the left dot. The current threshold several orders of magnitude smaller, marked by L2, indicates the onset of a cotunneling process where the right-dot energy level is aligned with the Fermi energy of the left electrode. Similarly, the Fermi level of the right electrode is aligned with the right (left) dot at the threshold line marked as line L3 (L4). The slopes of these threshold lines L1-L4, that is, -32, -54, 46, and 62, respectively, give α_i ($i = 1, 2, 3$) of 0.27, 0.19, and 0.54, respectively, at $V_{SD} \sim 0$. Figure 5(b) shows the effect of microwave irradiation on the resonant current peak. With increasing microwave power, satellite current peaks appear on the left (right) side of the main peak, owing to interdot tunneling upon the absorption (emission) of microwaves. Such microwave-assisted tunneling in a DQD has been observed in lateral and vertical dots [14,15]. At the satellite peak position, interdot detuning is equal to the microwave photon energy. Thus, the
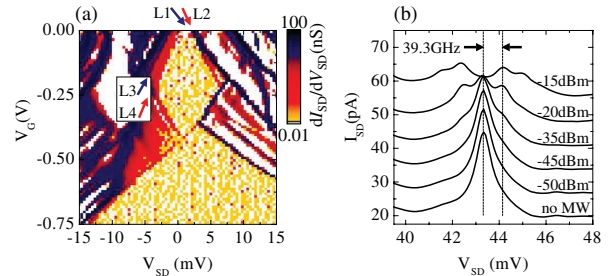
FIG. 4 (color). (a) Calculated differential conductance plotted as a function of $\epsilon_L - \epsilon_R$ and ϵ_L (normalized by Δ and $|g_L|\mu_B B$), where $2.5\Delta = 10\Omega = 1000\gamma_L = 100\gamma_R = \gamma$. Transport condition is categorized as two cases, I and II. We neglect a finite transition region between I and II due to small γ_L here. (b) Peak current in cases I and II as a function of normalized interdot coupling Ω/γ. Other parameters are the same as in (a).

FIG. 5 (color). (a) Logarithmic color scale dI_{SD}/dV_{SD} plot at 12 T. Four current threshold lines of the $N = 1$ Coulomb diamond are marked as L1-L4. The slopes of these lines gives the voltage drop ratio of the triple barrier, α_i ($i = 1, 2, 3$), for the low-V_{SD} region as 0.27, 0.19, and 0.54. (b) Resonant current peak under 39.3 GHz microwave. Interdot microwave-assisted tunneling is clearly apparent. Distance between the main and satellite peaks was used to estimate the interdot voltage drop ratio α_2 in high-V_{SD} regions as 0.193. The microwave powers are labeled for each trace. Each trace is shifted by a constant value.

distance between the main and the satellite peaks [marked as two dotted lines in Fig. 5(b)] gives α_2 of 0.193, which is close to the value for $V_{SD} \sim 0$. Similar values are obtained for different current peaks at different V_{SD}'s from 0 up to 100 mV, indicating that α_2 is independent of V_{SD}. On the other hand, voltage drop ratios for outer barriers α_i ($i = 1$, 3) are found to depend on V_{SD}. Indeed, in Fig. 1, the current threshold line from $N = 0$ at positive V_{SD} is not straight but bends upward. This indicates decreasing α_1 with increasing V_{SD}. As the slope of the current threshold lines is -12, as determined from Figs. 2(a)–2(d), α_1 at $V_{SD} \sim 35$ mV is smaller than α_1 at $V_{SD} \sim 0$ by 12/32. Thus, α_i ($i = 1, 2, 3$) is 0.10, 0.19, and 0.71, respectively, at $V_{SD} \sim 35$ mV [9]. Using these α_i's as well as the slope at $V_{SD} \sim 35$ mV, we obtain $|g_L|$ of 0.89 for our $In_{0.04}Ga_{0.96}As$ dot, and $|g_L - g_R|$ is 0.56. Thus, $|g_R|$ for our GaAs dot is 0.33 which is consistent with that obtained in the previous work on a vertical single dot with the same 10-nm-thick GaAs well [15]. The value of 0.89 for InGaAs seems to be large compared with the value obtained in the study of bulk $In_x Ga_{1-x}As$ [16], probably owing to the increasing density of In at the center of the well rather than at the InGaAs/AlGaAs interfaces, as is seen in the self-assembled InGaAs dot systems [17]. A stress in the thin InGaAs layer can be another possible reason for large g factor.

The width of the current peak in both regions A and D is ~ 0.5 mV in V_{SD}, and corresponds to ~ 0.1 meV using α_2. This width gives an upper bound for possible contributions from phonon-absorbing/emitting tunneling, and is smaller than the Zeeman energy difference in high magnetic field ($\gtrsim 10$ T). Thus, phonon absorption/emission for a misaligned spin sublevel in region B (C) in Fig. 3 is negligible. This point is also confirmed by a more detailed calculation, as in Fig. 3, where the phonon effects are included [12]. As depicted in the right inset of Fig. 1, there are some unoccupied levels located a few meV's below the aligned level in the right-dot. Thus, in addition to the RT through the two aligned levels, there is always a tunneling process with meV-phonon emission down to these low-lying levels. Such meV-phonon-emitting tunneling gives a background current of the order of ~ 10 pA, which defines the current threshold from the $N = 0$ region, as seen in Figs. 1 and 2(a)–2(d). RT current peak lines are also seen for negative V_{SD}. However, most of the peak widths are large, and no clear kink structure is observed. For negative V_{SD}, the direction of the $\Delta/2$ shift would be opposite, and δ_1 of the kink should be smaller as it is governed by the g factor of GaAs. This may be one of the reasons why we were not able to detect clear kink structures. In Fig. 2(d), there seems to be an additional line parallel to the current threshold line from the $N = 0$ region. We found that these lines, which appeared irregularly with some magnetic fields and V_{SD}'s, may be due to a fluctuation of the density of states in the electrode [18].

In conclusion, we measured the single electron transport through DQDs with different g factors. We found that the resonant tunneling is suppressed even when one of the Zeeman sublevels is aligned within the transport window. Finite level broadening of QD states partially relieves this bottleneck effect and gives a current peak when level detuning is half the Zeeman energy difference.

* k-ono@riken.jp

[1] *Semiconductor Spintronics and Quantum Computation* edited by D. D. Awschalom, N. Samarth, and D. Loss, (Springer-Verlag, Berlin, Germany, 2002).

[2] H. W. Jiang and E. Yablonovitch, Phys. Rev. B **64**, 041307 (2001); G. Salis *et al.*, Nature (London) **414**, 619 (2001); M. Poggio *et al.*, Phys. Rev. B **70**, 121305(R) (2004).

[3] D. Loss and D. P. DiVincenzo, Phys. Rev. A **57**, 120 (1998); D. P. DiVincenzo and D. Loss, J. Magn. Magn. Mater. **200**, 202 (1999).

[4] R. Hanson *et al.*, Rev. Mod. Phys. **79**, 1217 (2007).

[5] W. A. Coish and D. Loss, Phys. Rev. B **75**, 161302(R) (2007).

[6] E. A. Laird *et al.*, Phys. Rev. Lett. **99**, 246601 (2007); M. Pioro-Ladriere *et al.*, Nature Phys. **4**, 776 (2008).

[7] D. G. Austing *et al.*, Physica B (Amsterdam) **249–251**, 206 (1998).

[8] We observe significant decrease of I_{SD} at the field larger than 5T applied *parallel* to the wells, due to a field induced depletion at the outer tunneling barriers. F. Ancilotto *et al.*, Phys. Rev. B **67**, 205311 (2003).

[9] The electron density in the left electrode decreases due to the microfabrication, causing an offset of interdot detuning [7,10,11]. Decreased electron density leads to a thicker depletion layer in the gradiently n-doped electrode, thus increasing the effective barrier thickness. Weaker electron screening decreases the electric field inside the effective barrier. This asymmetry is further enhanced with large positive V_{SD}, as depicted in Fig. 1, right inset.

[10] K. Ono *et al.*, Physica B (Amsterdam) **314**, 450 (2002); S. Amaha *et al.*, Phys. Status Solidi C **5**, 174 (2008); C. Payette *et al.*, Physica E (Amsterdam) **40**, 1807 (2008); C. Payette *et al.*, Phys. Rev. Lett. **102**, 026808 (2009).

[11] K. Ono *et al.*, Science **297**, 1313 (2002); K. Ono and S. Tarucha, Phys. Rev. Lett. **92**, 256803 (2004); J. Baugh *et al.*, Phys. Rev. Lett. **99**, 096804 (2007).

[12] Y. Tokura *et al.*, Phys. Status Solidi B **246**, 740 (2009).

[13] S. A. Gurvitz and Ya. S. Prager, Phys. Rev. B **53**, 15932 (1996); T. H. Stoof and Yu. V. Nazarov, *ibid.* **53**, 1050 (1996).

[14] T. H. Oosterkamp *et al.*, Nature (London) **395**, 873 (1998).

[15] T. Kodera *et al.*, Physica E (Amsterdam) **22**, 518 (2004).

[16] C. Weisbuch and C. Hermann, Phys. Rev. B **15**, 816 (1977).

[17] N. Liu *et al.*, Phys. Rev. Lett. **84**, 334 (2000).

[18] L. P. Kouwenhoven *et al.*, Science **278**, 1788 (1997).